electrochem

MDPI

Article

Effect of Carbon Black, Carbon Nanotubes and Carbon Nanohorns on Electrochemical Performance of FeCoN/C Catalyst in Low Concentration Direct Ammonia Fuel Cells

Muhammad Javed Iqbal [1,*], Li-Wei Tseng [1], Fa-Cheng Su [2], Qaiser Abbas [1] and Hsiharng Yang [1,*]

[1] Graduate Institute of Precision Engineering, National Chung Hsing University, Taichung City 402, Taiwan; lawrence566565@gmail.com (L.-W.T.); qaiserastore@gmail.com (Q.A.)
[2] Industrial and Smart Technology Program, National Chung Hsing University, Nantou 540, Taiwan; fachengsu@dragon.nchu.edu.tw
* Correspondence: javedphd904@gmail.com (M.J.I.); hsiharng@nchu.edu.tw (H.Y.)

Abstract

Direct ammonia fuel cells (DAFCs) offer a promising pathway for carbon-free energy conversion but their practical performance is limited by sluggish cathode kinetics. In this work, non-precious FeCoN catalysts offer a cost-effective solution, yet carbon support optimization is crucial for activity and stability. FeCoN/XC-72R, FeCoN/CNT, and FeCoN/CNH cathode catalysts were synthesized by annealing at 550–750 °C. Their structure and morphology were analyzed by X-ray diffraction (XRD) and scanning electron microscopy (SEM). Electrochemical behavior was evaluated by cyclic voltammetry (CV) and electrochemical impedance spectroscopy (EIS) in alkaline medium containing KOH and NH_4OH. FeCoN/XC-72R exhibited the lowest resistance of 27 Ω and superior activity. In single cell tests using a 40 wt% PtIr/C anode catalyst at 2 mg cm^{-2}, the FeCoN/XC-72R catalyst achieved the highest power density of 71 mW/cm^2 under optimized conditions of 0.1M NH_4OH + 3M KOH, 100 °C, and O_2 feed. Among the carbon supports, carbon black (XC-72R) proved the most effective support for FeCoN catalysts in low concentration DAFCs, outperforming carbon nanotubes (CNTs) and carbon nanohorns (CNHs). These findings highlight the importance of carbon support selection in the design of efficient cathodes for next generation low concentration direct ammonia fuel cells.

Keywords: AEM-DAFC; direct ammonia fuel cell; carbon supports; non-precious metal catalyst; FeCoN/C; PtIr/C; M-N-C catalyst; carbon nanotubes; carbon black; carbon nanohorns

1. Introduction

Direct ammonia fuel cells (DAFCs) are gaining attention as promising clean energy devices because ammonia is carbon-free, contains a high hydrogen content, can be liquified under mild conditions, and is already supported by existing distribution infrastructure [1–4]. Compared with hydrogen, ammonia offers higher volumetric energy density, easier storage, transportation, and safety, which makes it an attractive fuel for decentralized power generation as well as portable and stationary applications [4–6]. In alkaline-membrane-based DAFCs, ammonia is oxidized at the anode, while oxygen is reduced at the cathode, producing electricity, with water and nitrogen as the main products under ideal operating conditions [7–10].

Received: 15 April 2026
Revised: 29 May 2026
Accepted: 9 June 2026
Published: 12 June 2026

Copyright: © 2026 by the authors. Licensee MDPI, Basel, Switzerland. This article is an open access article distributed under the terms and conditions of the Creative Commons Attribution (CC BY) license.

Despite these advantages, DAFCs still face major electrochemical and engineering challenges that limit practical use. The ammonia oxidation reaction at the anode is inherently slow and requires highly active and stable catalysts to reach useful current densities. More importantly, the oxygen reduction reaction (ORR) at the cathode remains a major bottleneck in both alkaline and anion exchange membrane DAFCs [11–16]. Conventional Platinum (Pt)-based catalysts remain the benchmark due to their excellent activity [17–20], but these catalysts are expensive and may lose performance because of ammonia crossover from the anode, which lowers cell voltage and durability. In addition, operation at a low ammonia concentration is preferred for safety, reduced crossover, and compatibility with dilute ammonia sources from industrial and agricultural streams [21–23]. However, these conditions also worsen kinetic limitations, decrease ionic conductivity, and increase mass transport resistance, creating a strong need for cathode catalysts with high intrinsic activity, good ammonia tolerance, and strong structural stability [22,24–27].

To address these challenges, non-precious metal-based cathode catalysts have emerged as promising candidates for platinum-free oxygen reduction in alkaline media [28,29]. These catalysts usually contain transition metals such as Ni, Co, Fe, Mo, and Mn coordinated with nitrogen species in conductive supports [30,31]. Among them, transition metal–nitrogen–support catalysts are the most promising platinum (Pt)-free electrocatalysts for alkaline environments. In particular, Fe-based catalysts have shown strong catalytic activity in fuel cells and can approach the performance of commercial Pt catalysts [32–35]. Their nitrogen doped active sites and metal–nitrogen coordination environments promote the preferred oxygen reduction reaction pathway and help suppress hydrogen peroxide formation, which is important because peroxide can damage the membrane and reduce electrode durability. During the synthesis, metal nanoparticles or clusters may also form and can further influence conductivity and catalytic performance [36–40].

The carbon support plays an important role in catalyst dispersion, electron transport, porosity, and resistance to corrosion [37,41–43]. Carbon black, especially Vulcan XC-72R, is widely used because of its low cost, high surface area, and easy processing, although its relatively low graphitization can make it more vulnerable to oxidation and structural degradation during long-term operation [44,45]. Carbon nanotubes provide one-dimensional conductive pathways, high electrical conductivity, and good mechanical strength, but their tendency to aggregate can reduce catalyst dispersion and limit electrolyte access [46–50]. Carbon nanohorns are a unique class of sp^2 carbon nanostructures made of horn-shaped graphene cones that self-assemble into spherical aggregates [51–56]. They offer a hierarchical pore network, a high defect density, and many anchoring sites for metal–nitrogen coordination, which may improve catalyst utilization and mass transport. Because these three supports differ in morphology, conductivity, porosity, and defect structure, the same FeCoN active phase may show different performances on each support [57].

This support effect is especially important in low concentration DAFCs, where the cathode must sustain efficient oxygen reduction under low ionic strength, slower reaction kinetics, and higher transport resistance [25,58–60]. A suitable support can improve the dispersion of metallic species, strengthen catalyst–carbon interactions, enhance charge transfer, and improve the access of oxygen and electrolyte to the active sites. In contrast, an unsuitable support can lead to poor active site utilization, higher resistance and lower durability. Therefore, comparing FeCoN catalysts supported on carbon black, carbon nanotubes, and carbon nanohorns is important for understanding how carbon architecture influences cathode performance in ammonia fuel cells [28,61–66].

In this study, FeCoN/C catalysts supported on XC-72R, CNTs, and CNHs were prepared and evaluated as cathode materials for low concentration DAFCs. The catalysts were synthesized by high temperature treatment under a nitrogen atmosphere to promote the

formation of well dispersed metal–nitrogen active sites and a conductive carbon framework, resulting in FeCoN/XC-72R, FeCoN/CNT, and FeCoN/CNH materials. Structural and electrochemical characterization was performed to examine the relationship between carbon support, catalyst morphology, and oxygen reduction behavior in alkaline media. In particular, X-ray diffraction, cyclic voltammetry, electrochemical impedance spectroscopy, and rotating disk electrode measurements were used to assess phase composition, catalytic activity, charge transfer resistance, and reaction kinetics. In addition, the effects of operating parameters, including electrolyte composition, and anode and cathode loading, were investigated to evaluate performance under low concentration ammonia conditions. This work aims to identify the most effective carbon support for FeCoN catalysts in AEM-DAFCs and to provide mechanistic insights into the role of support structures in determining electrochemical performances. The results are expected to support the rational design of low cost, efficient, and durable cathode catalysts for sustainable ammonia-based energy conversion systems.

2. Materials and Methods

All chemicals and materials were used as received, without further purification. The full details of the materials and characterization methods are provided in Supplementary Materials.

2.1. Surface Modification of Carbon Supports

The surface modification of carbon black by an acid treatment was performed following the previous reported method [67]. Carbon black (XC-72R) was reacted with 20% nitric acid in a reflux system at 110 °C for 12 h to introduce carboxylic and phenolic functional groups onto the carbon black surface, thereby enhancing its catalytic activity. After completion of the reaction, carbon black was separated by vacuum filtration and washed repeatedly with deionized water to remove the impurities and for pH neutralization. After washing, the carbon black was dried in an oven at 80 °C for 12 h to remove the moisture completely.

Carbon nanotubes required stronger oxidation treatment due to the hexagonal rigid structure and chemical inertness of CNTs. Carbon nanotubes were treated with a mixture of 70% concentrated nitric acid (HNO_3) and 95% sulfuric acid (H_2SO_4) in a 1:3 volume ratio [68]. The CNTs were refluxed in acidic solution at 120 °C under continuous stirring for 3 h to introduce the oxygen-containing functional groups at the surface, which play a critical role in improving interfacial interactions with metal catalysts. After acidification, the carbon nanotubes were thoroughly washed with DI water several times to neutralize the acid residue and filtered through vacuum filtration and dried at 80 °C for 12 h in an oven. After acid treatment, the modified carbon supports were stored in a vacuum desiccator for further use. Carbon nanohorns (CNHs) were used without acid treatment.

2.2. Preparation of FeCoN/C Cathode Catalyst

The FeCoN/C catalysts were synthesized by the 2-cyanoguanidine-assisted hydrothermal method by using three different carbon supports (carbon black (XC-72R), carbon nanotubes (CNTs) and carbon nanohorns (CNHs)). 2-Cyanoguanidine (1 g) was dissolved in deionized water (30 mL) and heated at 80 °C for 20 min. Subsequently, ferric chloride ($FeCl_3 \bullet 6H_2O$, 62 mg) and cobalt chloride ($CoCl_2 \bullet 6H_2O$, 80 mg) were then added, into the solution under continuous stirring for an additional 40 min at 80 °C. One of three functionalized carbon supports, XC-72R-COOH, CNT-COOH, or CNH, was introduced and dispersed with constant stirring and heating, followed by ultrasonic treatment to ensure the uniform distribution of metal precursor and carbon substrates. After that, the mixture

was filtered and dried at 90 °C for 12 h yielding a solid precursor powder. The dried powder was placed in a tube furnace under a nitrogen atmosphere and heated at 550 °C for 3 h, then raised to 750 °C for 1 h. This allowed the gaseous elements to effectively adhere to the material surface, resulting in the synthesis of FeCoN/XC-72R, FeCoN/CNT, and FeCoN/CNH cathode catalysts.

2.3. Catalyst Slurry Preparation

The gas diffusion layer used in this experiment had an area of 4.9 × 4.9 cm^2. Three different cathode catalysts, FeCoN/XC-72R, FeCoN/CNT, and FeCoN/CNH, were prepared, each with a loading of 1 mg/cm^2, 1.5 mg/cm^2 and 2 mg/cm^2. PtIr/C was used as an anode catalyst, with two loadings of 1 mg/cm^2 and 2 mg/cm^2. The catalyst ink was prepared by dispersing the solid catalyst into a mixed solution of deionized water (DI water), isopropyl alcohol (IPA), and an ionic polymer solution containing 5 wt% PiperION-A5. The ionic polymer helps establish an ion conduction channel between the catalyst layer and the AEM membrane, while IPA, acting as a dispersant, combined with DI water helps evenly disperse the catalyst powder.

2.4. Optimal Loading Test

The effects of different cathode catalyst loadings on fuel cell performance were studied. The catalyst (FeCoN/XC-72R, FeCoN/CNT, and FeCoN/CNH) loadings coated on cathode GDL are 1 mg/cm^2 to 1.5 mg/cm^2, 2 mg/cm^2 and 3 mg/cm^2 to identify the optimal configuration for achieving the highest power density. The anode catalyst used PtIr/C with a loading of 1–2 mg/cm^2 and the area of GDL was 4.9 × 4.9 cm^2.

2.5. Preparation of the Gas Diffusion Electrode (GDE)

The prepared catalyst slurry was evenly coated onto a 4.9 × 4.9 cm^2 carbon paper GDL-340 gas diffusion layer. Then, it was immersed in a 1M KOH solution for 48 h, and the KOH solution was replaced every 24 h to ensure successful activation. After activation, the single cell was assembled and its electrochemical performance was tested.

2.6. Activation of Anion Exchange Membrane

The anion exchange membrane PiperION-A20-HCO3 TP-85, is a high-performance membrane material suitable for anion exchange membrane direct ammonia fuel cells (AEM-DAFC). The membrane is mainly the condensation product of piperidine, terphenyl and 2,2,2-trifluoroacetophenone [69]. This material exhibits excellent anion conductivity, a wide range of chemical stability (pH 1–14), and an extremely thin membrane structure, making it highly promising in electrochemical applications such as alkaline fuel cells, alkaline electrolyzers and direct ammonia fuel cells. The PiperION-A20-HCO3 TP-85 anion exchange membrane was cut into 6 × 6 cm^2 squares. The membrane was then immersed in a 0.5 M potassium hydroxide (KOH) solution for 2 h to convert the hydroxide (OH^-) form, thereby improving the membrane's conductivity and electrochemical reactivity. Once the conversion was completed, the single cell assembly and subsequent performance was tested.

3. Results and Discussion

Acid treatment effectively modifies the surfaces of carbon nanotubes and carbon black by introducing oxygen-containing functional groups, thereby increasing the number of active sites for metal coordination. These surface modifications markedly increase the dispersibility in aqueous media. As a result, acid-functionalized carbon black and carbon nanotubes showed excellent dispersibility, whereas their unmodified counterparts remained poorly dispersible. Additionally, the carbon nanohorns were used without

acid modification because carbon nanohorns were easily dispersed in deionized water (Figure S1). The hydrophilic character of untreated and modified carbon black and carbon nanotubes were analyzed by a water contact angle as shown in Figure S2.

FTIR spectroscopy was used to investigate the surface functional groups of XC-72R carbon black and CNTs before and after acid treatment. Carbon black (XC-72R) exhibits a broad band at 3850–3600 cm^{-1}, which can be assigned to O-H stretching. The bands near 2920–2860 cm^{-1} are attributed to aliphatic C-H stretching and the band near 2675 cm^{-1}, corresponding to the presence of quaternary ammonium (N-H). The absorption features in the 2021–1744 cm^{-1} region are associated with a carbonyl-containing species, including C = O stretching from carboxyl moieties, whereas the band near 1542 cm^{-1} is associated with aromatic C = C skeleton vibrations. The region between 1198 and 1032 cm^{-1} is characteristic of C-O stretching and the signals near 1013–856 cm^{-1} arise from bending vibrations of aromatic C-H. The acid treatment, intensification of the oxygen-containing bands and appearance of additional features in the region of 2104–1542 cm^{-1} range indicate successful surface oxidation and the generation of more defect-related functional groups [70,71]. The transmittance values presented in the FTIR spectra are unnormalized (Figure 1a,b). The spectral changes indicate that the acid treatment enriches the carbon black surface with nitrogen, oxygen, and unsaturated carbon functionalities. Similarly changes in the surface functional groups of carbon nanotubes before and after acid functionalization were also evaluated by Fourier transform infrared (FTIR) spectroscopy. The FTIR spectrum of untreated CNT showing the weak signals, indicating a very low density of surface functional groups, on graphitized carbon. After modification, significant absorption peaks appeared at 3687–3217 cm^{-1}, which were assigned to the O-H stretching vibrations of hydroxyl and carboxylic groups. The bands at 2961 and 2871 cm^{-1} correspond to aliphatic C-H stretching, while the peak at 1825 cm^{-1} is attributed to the C = O stretching of carbonyl species. The bands near 1690–1558 cm^{-1} can be assigned to C = O stretching and aromatic C = C skeletal vibrations indicating oxidation and the formation of defects. In addition, the peaks at 885–798 cm^{-1} are consistent with the bending vibrations of aromatic C-H (Figure 1b) [72–75]. Similarly, the FTIR spectrum of the carbon nanohorns is shown in Figure S3. These spectral changes demonstrate that acid treatment effectively introduces oxygen-containing functional groups.

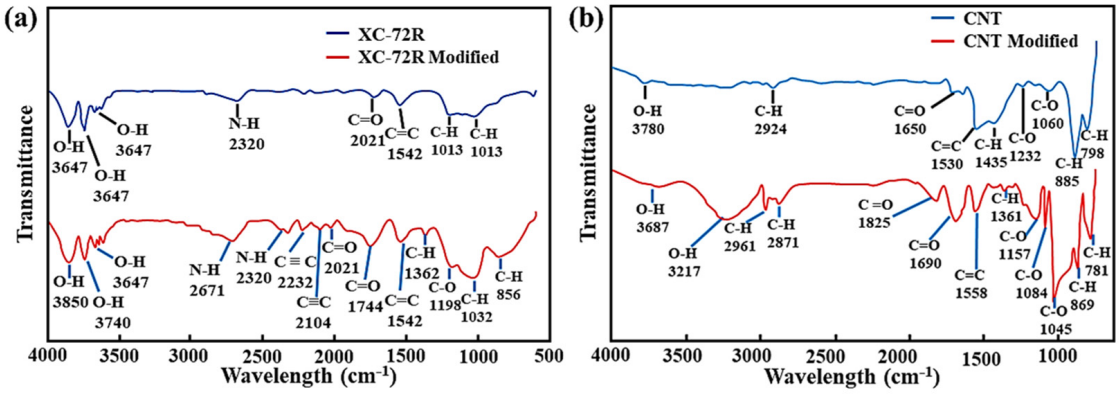


Figure 1. FTIR spectra of carbon supports before and after modification; (**a**) carbon black (XC-72), (**b**) CNTs.

The FeCoN/C catalysts supported on XC-72R, CNTs and CNHs were prepared by a hydrothermal process followed by annealing at 550 °C and 750 °C (Figure 2). The choice of carbon support affected the resulting catalyst's properties through differences in surface chemistry and morphology, which likely influenced precursor adsorption and thermal evolution during pyrolysis. The resulting materials labeled FeCoN/XC-72R, FeCoN/CNT,

and FeCoN/CNH exhibited different structural and electrochemical properties depending on nature of the carbon support. The synthesis strategy combines precursor chemistry with rational support selection to control catalyst formation and finally tune the properties of FeCoN-based materials for fuel cell Applications.

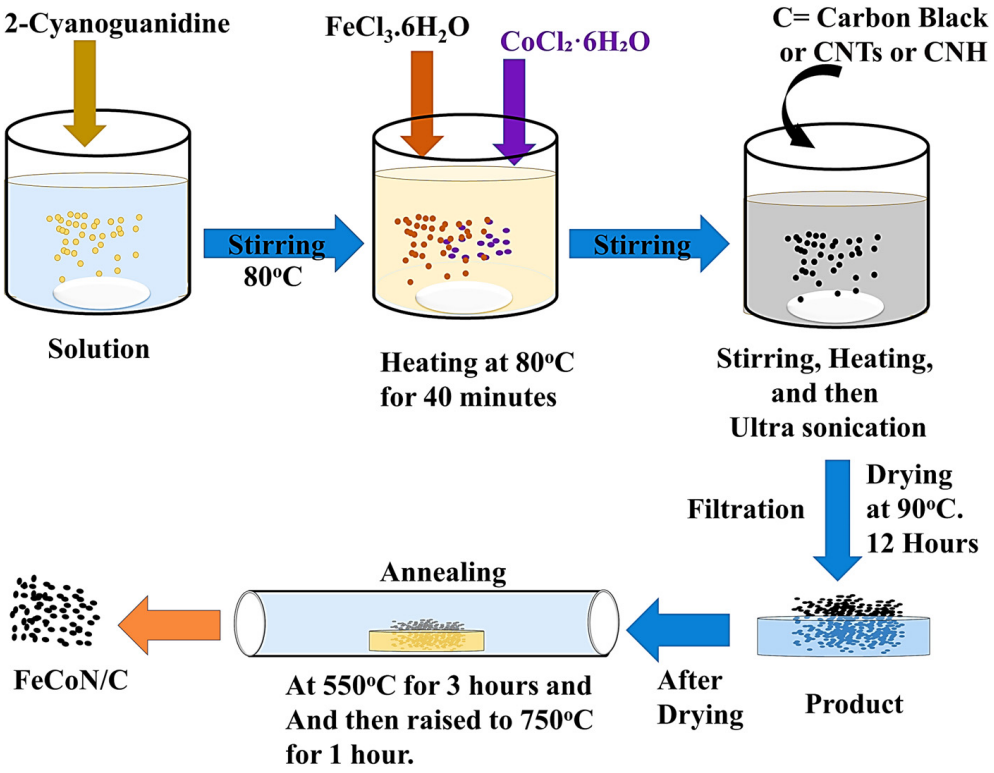


Figure 2. Schematics for the synthesis of FeCoN/XC-72R, FeCoN/CNT, and FeCoN/CNH cathode catalysts.

The surface morphologies of FeCoN/XC-72R, FeCoN/CNT, and FeCoN/CNH were observed by scanning electron microscopy (SEM) at 30 K and 50 K magnification to evaluate the influence of carbon support on catalyst formation and dispersion. All samples were annealed under a nitrogen atmosphere in a tube furnace to promote precursor conversion and catalyst formation. FeCoN/XC-72R exhibited a relatively uniform distribution of nanoscale FeCoN particles across the carbon black framework. The surface defects and functional group present on XC-72R likely facilitated the anchoring of the active species, yielding a homogeneous coating without significant particle agglomeration (Figure 3a,b). FeCoN/CNT showed a tubular network morphology, with FeCoN nanoparticles decorated on the CNT surface and in some regions, bridging adjacent tubes (Figure 3c,d). This one-dimensional conductive structure may favor electron transport along the axial direction; however, some localized particle clustering at tube junctions could reduce the accessibility of certain active sites. FeCoN/CNH displayed canonical nanohorns like architecture, with FeCoN particles distributed over the outer surfaces and in the interstitial spaces between the horns (Figure 3e,f). This morphology increases the surface roughness and may provide more available sites for catalyst deposition. The high curvature of CNHs may also promote stronger interactions with supported species and improve gas–solid contact, which can be beneficial for catalytic reactions. Across all supports, no obvious large scale phase separation was observed, indicating that the high temperature pyrolysis under nitrogen effectively immobilized FeCoN species, while preserving the carbon nanostructures. The observed morphological differences highlight the important role of carbon support topology in controlling catalyst dispersion, surface accessibility, and likely mass transport behavior,

all of which can influence the electrochemical performance of direct ammonia fuel cells. Further EDS analysis of the weight percentages of the catalyst (Table S1) confirms that the experimental synthesis results closely align with the designed composition (Figure S4), thereby verifying the successful fabrication of the targeted cathode catalyst. BET analysis before and after the treatment of carbon black and carbon nanotubes was performed, which showed that treated carbon black and carbon nanotubes exhibited greater surface areas. Nitrogen (N_2) adsorption isotherms of carbon supports are as shown in Figure S5.

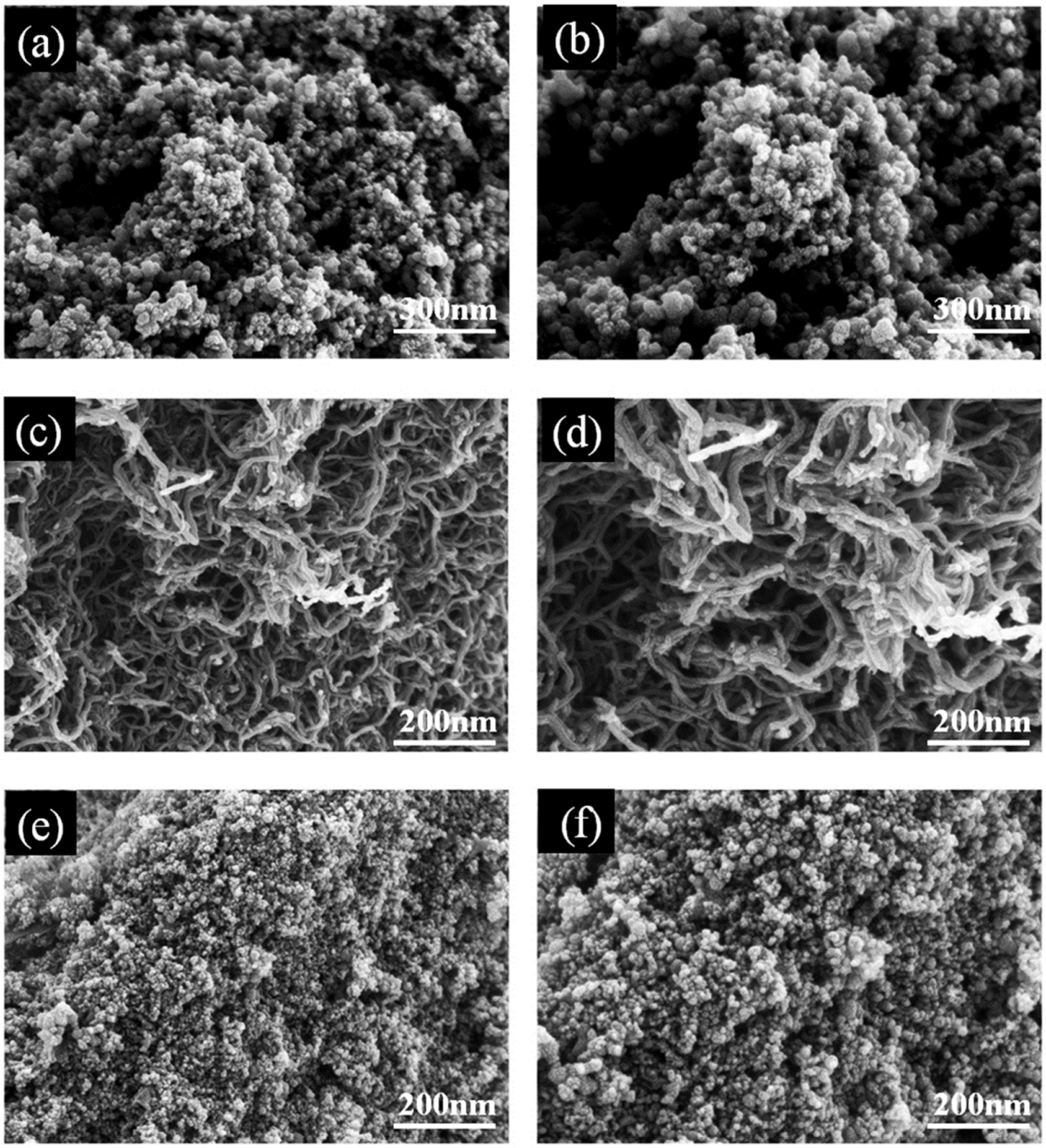


Figure 3. Surface morphologies of (**a**,**b**) FeCoN/XC-72R, (**c**,**d**) FeCoN/CNT, (**e**,**f**) and FeCoN/CNH.

X-ray diffraction was employed to identify the crystalline phases and assess the structural evaluation of a FeCo-based cathode catalyst supported on XC-72R, CNT and CNHs. All samples exhibited the characteristic diffraction peaks of graphitic carbon at two theta (2θ) values 26.2–26.5°, 42–43.0° and 78–79.5°, which can be indexed to the (002), (101) and (110) planes respectively, according to the JCPDS No. 41-1487. These reflections indicate the preserved graphitic structure of the carbon supports, with variations in peak intensity and breadth reflecting differences in graphitization and structural order among

XC-72R, CNTs, and CNHs. In addition, distinct peaks at two theta (2θ) values of 43.8–44.6° and 64.9–66.5° were observed and assigned to the (110) and (200) planes of the CoFe alloy phase respectively, in agreement with the JCPDS No. 49-1568 (Figure 4a–c). The presence of these reflections confirms the formation of FeCoN during high temperature annealing. The similar relative intensity of alloy peaks across all the samples suggests comparable alloy crystallinity, while slight peak broadening indicates nanoscale crystalline dimensions. In this work, nitrogen is introduced from 2-cyanoguanidine during pyrolysis and is expected to contribute to the chemical environment of the catalyst by promoting nitrogen doping and a possible metal–nitrogen network in the matrix. However, such nitrogen-related species are typically difficult to identify directly by XRD because they are often amorphous, highly dispersed or below the detection limit of the technique. Therefore, the XRD results mainly support the formation of graphitic carbon and FeCo alloy phases, rather than directly confirming FeCoN. The absence of separate Fe or Co oxide reflections suggests that annealing under the nitrogen atmosphere favored reduction and alloy formation, but it does not exclude the possible presence of amorphous or highly dispersed oxide species below the XRD detection limit. The XRD pattern indicates that the FeCoN catalysts were successfully formed on all three carbon supports, while the preserved graphitic carbon structure should help maintain electrical conductivity and provide a suitable framework for catalyst integration.

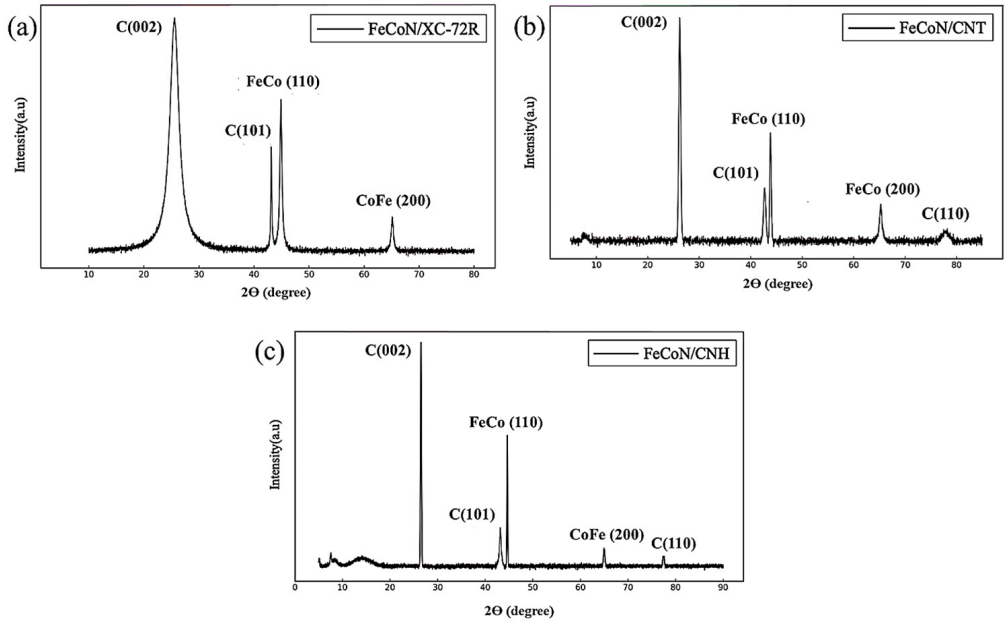


Figure 4. XRD analysis of (**a**) FeCoN/XC-72R, (**b**) FeCoN/CNT, and (**c**) FeCoN/CNH.

The electrochemical performance of FeCoN catalysts supported on carbon black XC-72R, CNT, CNH were evaluated by cyclic voltammetry (CV) in 0.1M NH_4OH and 3M KOH using a Hg/HgO reference electrode (Figure 5a). The measurements were conducted over a potential range of −1.0 to 0.5 V at the scan rate of 20 mVs^{-1}. All three catalysts exhibited well-defined redox responses, indicating the presence of electrochemically active surface sites associated with the FeCoN phase. Among three catalysts, FeCoN/CNH showed the smallest voltametric loop area and lower peak current density, suggesting lower electrochemical activity and less favorable charge transfer behavior under tested conditions. In contrast, FeCoN/XC-72R and FeCoN/CNT demonstrated larger loop areas and higher current responses, which may reflect improved electrochemical accessibility and more efficient interfacial charge transport.

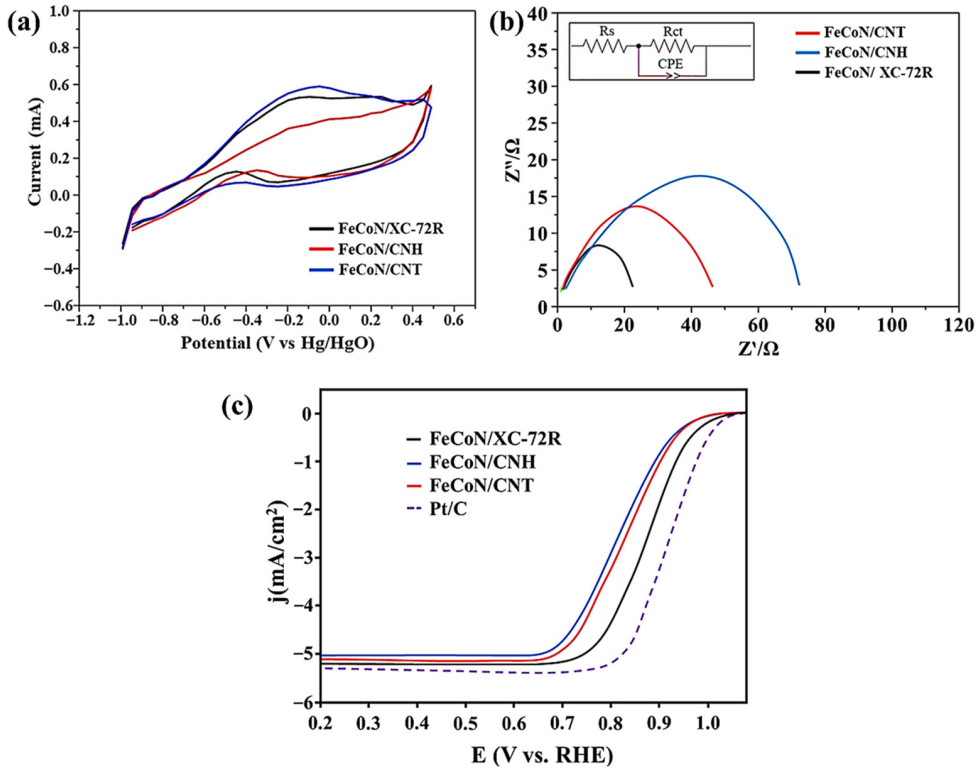


Figure 5. Electrochemical analysis of FeCoN/XC-72R, FeCoN/CNT and FeCoN/CNH catalysts; (**a**) CV, (**b**) EIS, (**c**) polarization curves of FeCoN on different carbon supports for ORR in O_2-saturated 0.1M KOH at 2400 rpm with a scan rate of 10 mVs^{-1} RDE.

The superior response of FeCoN/XC-72R and FeCoN/CNT may be related to differences in support morphology and surface structure. Greater functionality of carbon black XC-72R can promote the better dispersion of the active phase and provide more accessible catalytic sites, while the curved and conical architecture of CNHs may also facilitate reactant access and catalyst utilization.

Electrochemical impedance spectroscopy (EIS) was used to investigate the charge transfer characteristics of FeCoN catalysts supported on XC-72R, CNTs, and CNHs. EIS was conducted over a frequency range of 100 kHz to 0.1 Hz with a 5 mV amplitude, and acquired results were fitted using an appropriate equivalent circuit. The Nyquist plots were fitted using the equivalent circuit R_s-(R_{ct} || CPE), where R_s represents the solution resistance, R_{ct} represents the charge transfer resistance associated with the oxygen reduction reaction (ORR), and the constant phase element (CPE) accounts for non-ideal capacitive behavior arising from surface heterogeneity. Among the three catalysts, FeCoN/XC-72R demonstrated the lowest total resistance of 27 Ω, compared with 56 Ω for FeCoN/CNT and 87 Ω for FeCoN/CNH as shown in Figure 5b. This lower resistance suggests faster interfacial electron transfer and more efficient ion transport for the XC-72R-supported catalyst under operating conditions. The lower resistance of FeCoN/XC-72R is consistent with its stronger CV response and suggests that this support provides a more favorable electrochemical environment for catalyst utilization. This behavior may be associated with surface functionalization and the dispersion of XC-72R, which can improve active site accessibility and reduce interfacial resistance. The ORR polarization curves of FeCoN-based catalysts supported on modified carbon black, CNTs and CNHs were measured in O_2-saturated 0.1M KOH (Figure 5c). Among these catalysts, FeCoN/XC-72R showed more positive onset potential with higher cathodic current density, indicating the superior ORR activity as compared to the other synthesized catalysts.

The influence of carbon supports (XC-72R, CNTs and CNHs) on the performance of the FeCoN cathode catalysts was evaluated in alkaline direct ammonia fuel cells under the same operating conditions. The anode fuel consisted of 0.1M NH_4OH + 3M KOH, while oxygen was supplied to the cathode. All the measurements were performed at 100 °C using 5 wt% PiperION-A5 ionomer. The catalyst inks were uniformly coated onto gas diffusion layers (GDLs, 4.9 × 4.9 cm^2) and assembled into single cells with a cathode loading of 1 mg/cm^2 FeCoN and PtIr/C anode loading of 1 mg/cm^2. Among the three catalysts, FeCoN/XC-72R delivered the highest peak density of 45 mW/cm^2, compared with 39 mW/cm^2 for FeCoN/CNT and 32 mW/cm^2 for FeCoN/CNH (Figure 6a). This result indicates that the XC-72R-supported catalyst provided the most favorable cell performance under the tested conditions. The superior performance of the FeCoN/XC-72R catalyst is broadly consistent with the electrochemical impedance and cyclic voltammetry results, in which FeCoN/XC-72R exhibited the lowest resistance (27 Ω) and most favorable electrochemical response. This improved performance may be related to differences in support morphology, surface chemistry, and catalyst dispersion, which can affect the charge transport and reactant accessibility. The findings establish XC-72R as a highly effective support for FeCoN-based cathode catalysts in alkaline ammonia fuel cells.

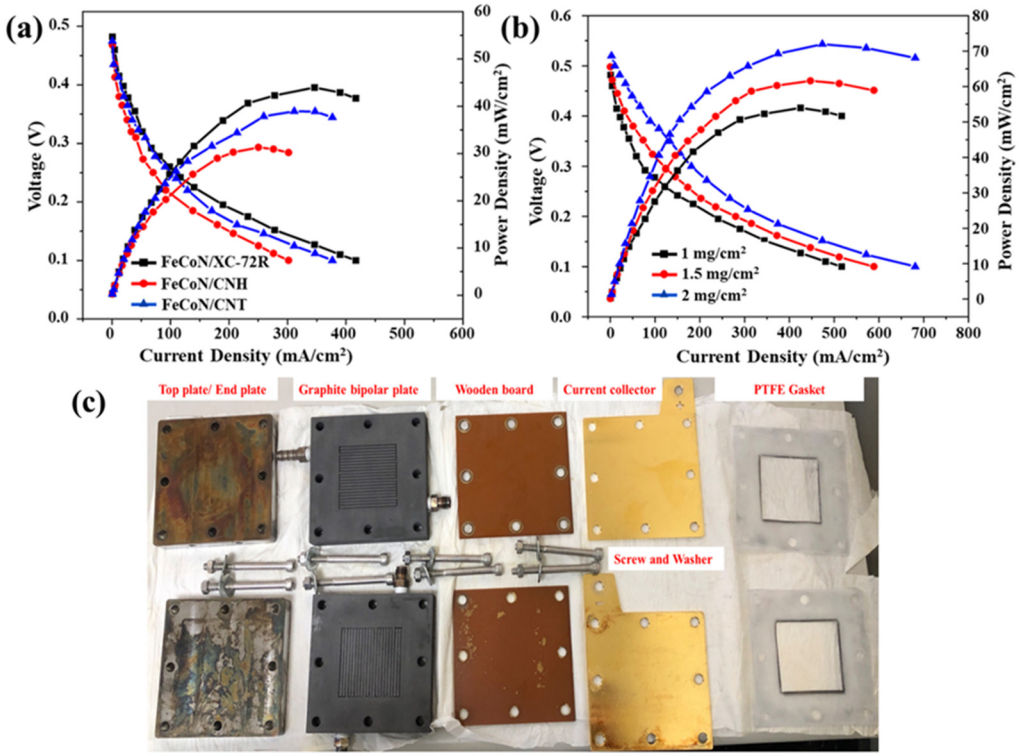


Figure 6. Comparison of power density of (**a**) FeCoN catalysts with different carbon supports; (**b**) optimization of cathode catalyst with different loadings (**c**) ammonia fuel cell assembly used for performance tests.

The power density of the ammonia fuel cell was improved by fine tuning both the anode and cathode catalyst loadings. Building on the optimized FeCoN/XC-72R cathode catalyst, the loading at the cathode was increased from 1 mg/cm^2 to 2 mg/cm^2, while the PtIr/C anode loading was kept at 2 mg/cm^2. Fuel cell performance was evaluated using 0.1M NH_4OH and 3M KOH at the anode and oxygen at the cathode, at 100 °C with 5 wt% PiperION-A5 ionomer, and a 4.9 × 4.9 cm^2 active area. The increase in cathode catalyst loading significantly enhanced the power density, rising from 45 mW/cm^2 at 1 mg/cm^2 with a PtIr/C loading of 1 mg/cm^2 to 71 mW/cm^2 at 2 mg/cm^2 loading of both

anode (PtIr/C) and cathode catalysts (Figure 6b). This improvement can be attributed to the higher catalyst loading increasing the number of accessible active sites and the reduced local kinetic limitations at the cathode. The performance gain may also be influenced by overall electrode composition, although the individual contributions of the cathode and anode loading cannot be separated from the present data. These results indicate that catalyst loading is an important parameter for improving cell performance in low concentration ammonia fuel cells, while further optimization would still be needed to determine the practical loading limit. Single cell ammonia fuel cell assembly for the single cell used in tests is shown in Figure 6c. The performance of the developed cathode catalyst (FeCoN/XC-72R) was evaluated; a comparative fuel cell test was performed using commercial Pt/C and PtIrC anode catalyst under the same loading and optimized operating conditions. The PtIr/C anode catalyst showed better overall cell performance than Pt/C under optimized conditions (Figure S9). The similar performances of FeCoN/CNH and FeCoN/XC-72R at low current densities may be attributed to their comparable catalyst utilization and reaction kinetics under mild operation conditions. Although the two carbon supports differ in morphology and surface structure, these differences appear to have a limited effect at low current, where the overall activity is mainly governed by the intrinsic catalytic behavior of FeCoN active sites. At higher current densities, the influence of the support structure becomes more pronounced, which may account for the divergence observed in the cell performance.

The operational durability of the optimized FeCoN/XC-72R cathode was evaluated under accelerated cycling conditions in a single cell configuration. PtIr/C with a loading of 2.0 mg/cm^2 was used as the anode, and FeCoN/XC-72R with a catalyst loading of 2.0 mg/cm^2 was used as the cathode. The anode was supplied with 0.1M NH_4OH + 3M KOH, while oxygen served as the cathode oxidant. The fuel cell setup used for testing is shown in Figure 7a. The tests were conducted at 100 °C, and the cell was operated under constant conditions for 50 h before the performance assessment. The peak power density decreased from 71 mW/cm^2 to 48.98 mW/cm^2, corresponding to an absolute loss of 22.02 mW/cm^2 and relative decrease of approximately 31% (Figure 7b). This decline suggests a partial performance degradation of the FeCoN/XC-72R cathode during cycling. Possible contributors include catalyst layer restructuring, the loss of active site accessibility, support degradation or changes in electrodes under prolonged operations. While the FeCoN/XC-72R cathode showed a promising initial performance, durability results indicated that further optimization was still needed to improve long-term stability for practical low concentration direct ammonia fuel cell applications.

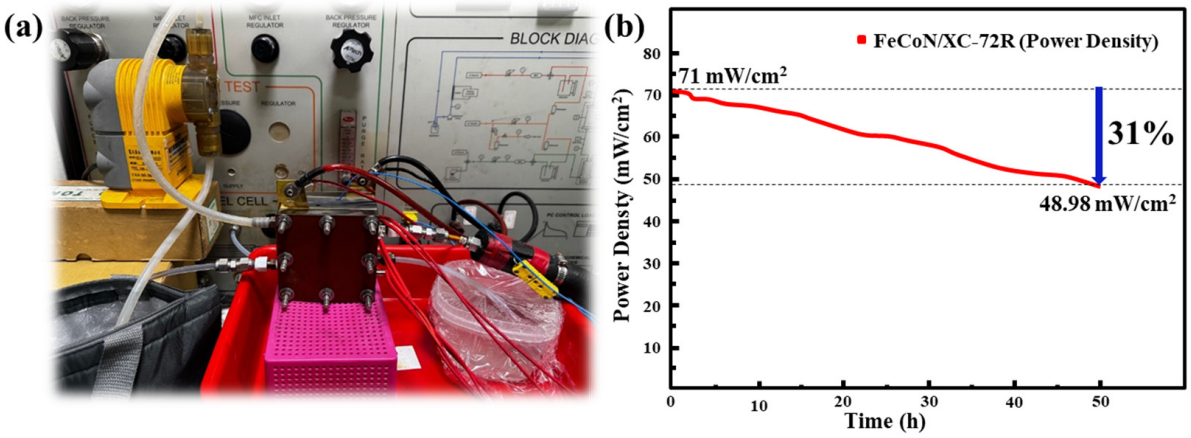


Figure 7. (**a**) Fuel cell setup; (**b**) FeCoN/XC-72R fuel cell stability test.

Compared with the reference catalysts listed in Table 1, the FeCoN/XC-72R-catalyst-based cell showed a competitive power density of 71 mW/cm^2 under low fuel concentration conditions. Although the catalyst composition and testing conditions differ among the reported systems, the present work highlights the effectiveness of the carbon support-based design, particularly the use of acid-functionalized XC-72R, and CNTs in improving catalyst utilization and overall cell performance.

Table 1. Fuel cell power density comparison chart.

Fuel Concentration	Anode Loading (mg/cm^2)	Cathode Loading (mg/cm^2)	Temperature (°C)	Membrane	Peak Power Density (mW cm^{-2})	Ref.
0.5 M NH_4OH + 0.5 M KOH	Pt cubes$_{H-S}$ 2 mg/cm^2	Pt black	50	AEM (PVBC)	42.4	[76]
0.2 M NH_3 + 1 M KOH	Pt/C 0.6 mg/cm^2	Pt/C 0.6 mg/cm^2	80	HEM (AHA)	0.22	[77]
0.1M $NH_3{\cdot}H_2O$ + 3M KOH	PtRu/C 4.5 mg/cm^2	Pd/C 2 mg/cm^2	80	AEM	3	[78]
0.1M NH_4OH + 3M KOH	PtIr/C 2 mg/cm^2	FeCoN/XC-72R 2 mg/cm^2	100	AEM	71	This Work

4. Conclusions

In this study, the FeCoN cathode catalysts supported on XC-72R, CNTs, and CNHs were successfully synthesized and evaluated for low concentration direct ammonia fuel cells. The choice of carbon support was found to strongly influence the morphology, electrochemical response, and fuel cell performance of the catalysts. Among the three catalysts, FeCoN/XC-72R showed superior performance, with the lowest resistance, a stronger electrochemical response and the highest peak power density after optimization of the catalyst loading. Increasing the FeCoN/XC-72R cathode loading to 2 mg/cm^2 improved the peak power density to 71 mW/cm^2 under 0.1M NH_4OH + 3M KOH. These results indicate that carbon support selection and catalyst loading are important parameters in determining cell performance. However, the durability test also showed a noticeable decline in stability, highlighting the need for further improvement before practical application.

Supplementary Materials: The following supporting information can be downloaded at: https://www.mdpi.com/article/10.3390/electrochem7020014/s1.

Author Contributions: M.J.I.: Conceptualization, methodology, writing—original draft, review and editing. L.-W.T.: Investigation, data curation, and formal analysis. F.-C.S.: Investigation, formal analysis and validation. Q.A.: Investigation, data curation and formal analysis. H.Y.: Principal investigator, supervision, conceptualization, methodology, writing, review and editing, validation, and funding acquisition. All authors have read and agreed to the published version of the manuscript.

Funding: This research was funded by the National Science and Technology Council of Taiwan, under project grant numbers NSTC 113-2221-E-005-077-MY3 and NSTC 113-2634-F-005-002.

Institutional Review Board Statement: Not applicable.

Informed Consent Statement: Not applicable.

Data Availability Statement: The original contributions presented in this study are included in the article/Supplementary Material. Further inquiries can be directed to the corresponding author.

Acknowledgments: The authors acknowledge the National Chung Hsing University for their support. This research was supported by, Sustainable New Agriculture Research Center (SMARTer), and Ministry of Education, Taiwan, under the Higher Education Sprout Project.

Conflicts of Interest: The authors declare the following financial interests, which may be considered as potential competing interests: Hisharng Yang reports financial support provided by the National

Science and Technological council (NSTC). All other authors declare that they have no known competing financial or personal interests that could have appeared to influence this work.

References

1. Han, Y.; Zhao, Y.; Ren, Z.; Wei, T.; Zhang, H.; Sun, S.; Yu, H.; Shao, Z. Studies on ammonia crossover behavior of hydroxide exchange membranes for direct ammonia fuel cells. *J. Membr. Sci.* **2025**, *717*, 123638. [CrossRef]
2. Abbasi, R.; Setzler, B.P.; Wang, J.; Zhao, Y.; Wang, T.; Gottesfeld, S.; Yan, Y. Low-temperature direct ammonia fuel cells: Recent developments and remaining challenges. *Curr. Opin. Electrochem.* **2020**, *21*, 335–344. [CrossRef]
3. Metkemeijer, R.; Achard, P. Ammonia as a feedstock for a hydrogen fuel cell; reformer and fuel cell behaviour. *J. Power Sources* **1994**, *49*, 271–282. [CrossRef]
4. Miyaoka, H.; Miyaoka, H.; Ichikawa, T.; Ichikawa, T.; Kojima, Y. Highly purified hydrogen production from ammonia for PEM fuel cell. *Int. J. Hydrogen Energy* **2018**, *43*, 14486–14492. [CrossRef]
5. Wen, Z.; Huang, B.; Wang, Y.; Wang, K.; Tu, X.; Xie, P.; Fu, X. Ammonia as a renewable energy carrier from synthesis to utilization. *Nat. Rev. Clean Technol.* **2025**, *1*, 755–770. [CrossRef]
6. Tan, H.; Sang, Z.; Tian, Y.; Peng, W.; Liu, X.; Liang, J. Ammonia as a green carbon-free fuel: A pathway to the sustainable energy economy. *ACS Energy Lett.* **2024**, *9*, 5120–5136. [CrossRef]
7. Lan, R.; Tao, S. Direct ammonia alkaline anion-exchange membrane fuel cells. *Electrochem. Solid-State Lett.* **2010**, *13*, B83–B86. [CrossRef]
8. Li, Y.; Pillai, H.S.; Wang, T.; Hwang, S.; Zhao, Y.; Qiao, Z.; Mu, Q.; Karakalos, S.; Chen, M.; Yang, J. High-performance ammonia oxidation catalysts for anion-exchange membrane direct ammonia fuel cells. *Energy Environ. Sci.* **2021**, *14*, 1449–1460. [CrossRef]
9. Hren, M.; Božič, M.; Fakin, D.; Kleinschek, K.S.; Gorgieva, S. Alkaline membrane fuel cells: Anion exchange membranes and fuels. *Sustain. Energy Fuels* **2021**, *5*, 604–637. [CrossRef]
10. Siddiqui, O.; Dincer, I. Investigation of a new anion exchange membrane-based direct ammonia fuel cell system. *Fuel Cells* **2018**, *18*, 379–388. [CrossRef]
11. Ramaswamy, N.; Mukerjee, S. Alkaline anion-exchange membrane fuel cells: Challenges in electrocatalysis and interfacial charge transfer. *Chem. Rev.* **2019**, *119*, 11945–11979. [CrossRef] [PubMed]
12. Chatterjee, S.; Parsapur, R.K.; Huang, K.-W. Limitations of ammonia as a hydrogen energy carrier for the transportation sector. *ACS Energy Lett.* **2021**, *6*, 4390–4394. [CrossRef]
13. He, Q.; Cairns, E.J. Recent progress in electrocatalysts for oxygen reduction suitable for alkaline anion exchange membrane fuel cells. *J. Electrochem. Soc.* **2015**, *162*, F1504–F1539. [CrossRef]
14. Cai, A.; Rozario, Z. Direct Ammonia Fuel Cells: A general overview, current technologies and future directions. *Johns. Matthey Technol. Rev.* **2022**, *66*, 479–489. [CrossRef]
15. Asmare, M.; İlbaş, M. Direct ammonia fueled solid oxide fuel cells: A comprehensive review on challenges, opportunities and future outlooks. *Int. J. Energy Technol.* **2020**, *2*, 70–91. [CrossRef]
16. Dhawale, D.S.; Biswas, S.; Kaur, G.; Giddey, S. Challenges and advancement in direct ammonia solid oxide fuel cells: A review. *Inorg. Chem. Front.* **2023**, *10*, 6176–6192. [CrossRef]
17. Ehelebe, K.; Schmitt, N.; Sievers, G.; Jensen, A.W.; Hrnjic, A.; Collantes Jiménez, P.; Kaiser, P.; Geuß, M.; Ku, Y.-P.; Jovanovic, P.; et al. Benchmarking fuel cell electrocatalysts using gas diffusion electrodes: Inter-lab comparison and best practices. *ACS Energy Lett.* **2022**, *7*, 816–826. [CrossRef]
18. Pedersen, C.M.; Escudero-Escribano, M.; Velázquez-Palenzuela, A.; Christensen, L.H.; Chorkendorff, I.; Stephens, I.E. Benchmarking Pt-based electrocatalysts for low temperature fuel cell reactions with the rotating disk electrode: Oxygen reduction and hydrogen oxidation in the presence of CO. *Electrochim. Acta* **2015**, *179*, 647–657. [CrossRef]
19. Riasse, R.; Lafforgue, C.; Vandenberghe, F.; Micoud, F.; Morin, A.; Arenz, M.; Durst, J.; Chatenet, M. Benchmarking proton exchange membrane fuel cell cathode catalyst at high current density: A comparison between the rotating disk electrode, the gas diffusion electrode and differential cell. *J. Power Sources* **2023**, *556*, 232491. [CrossRef]
20. Huang, L.; Zaman, S.; Tian, X.; Wang, Z.; Fang, W.; Xia, B.Y. Advanced platinum-based oxygen reduction electrocatalysts for fuel cells. *Acc. Chem. Res.* **2021**, *54*, 311–322. [CrossRef]
21. Jeerh, G.; Zhang, M.; Tao, S. Recent progress in ammonia fuel cells and their potential applications. *J. Mater. Chem. A* **2021**, *9*, 727–752. [CrossRef]
22. Wang, Y.-H.; Gao, F.-Y.; Zhang, X.-L.; Yang, Y.; Liao, J.; Niu, Z.-Z.; Qin, S.; Yang, P.-P.; Yu, P.-C.; Sun, M. Efficient NH3-tolerant nickel-based hydrogen oxidation catalyst for anion exchange membrane fuel cells. *J. Am. Chem. Soc.* **2023**, *145*, 17485–17494. [CrossRef]
23. Adli, N.M.; Zhang, H.; Mukherjee, S.; Wu, G. Ammonia oxidation electrocatalysis for hydrogen generation and fuel cells. *J. Electrochem. Soc.* **2018**, *165*, J3130–J3147. [CrossRef]

24. Wu, Z.; Wang, Y.; Cao, Y.; Wang, B.; Sun, Z.; Yang, J.; Li, Y. Ammonia tolerance of atomically dispersed single metal site catalysts: Mechanistic understanding and high-performance oxygen reduction electrocatalysis. *Adv. Funct. Mater.* **2023**, *33*, 2301084. [CrossRef]
25. He, Y.; Liu, S.; Priest, C.; Shi, Q.; Wu, G. Atomically dispersed metal–nitrogen–carbon catalysts for fuel cells: Advances in catalyst design, electrode performance, and durability improvement. *Chem. Soc. Rev.* **2020**, *49*, 3484–3524. [CrossRef]
26. Li, W.; Liu, Y.; Luo, M.; Shi, X.; Pan, Z.; Chen, R.; An, L. Monitoring ammonia and water transport through anion exchange membranes in direct ammonia fuel cells. *J. Power Sources* **2025**, *628*, 235900. [CrossRef]
27. Burns, M.; Qin, M. Ammonia recovery from organic nitrogen in synthetic dairy manure with a microbial fuel cell. *Chemosphere* **2023**, *325*, 138388. [CrossRef]
28. Wu, G.; More, K.L.; Johnston, C.M.; Zelenay, P. High-performance electrocatalysts for oxygen reduction derived from polyaniline, iron, and cobalt. *Science* **2011**, *332*, 443–447. [CrossRef]
29. Shao, M.; Chang, Q.; Dodelet, J.-P.; Chenitz, R. Recent advances in electrocatalysts for oxygen reduction reaction. *Chem. Rev.* **2016**, *116*, 3594–3657. [CrossRef] [PubMed]
30. Lefèvre, M.; Proietti, E.; Jaouen, F.; Dodelet, J.-P. Iron-based catalysts with improved oxygen reduction activity in polymer electrolyte fuel cells. *Science* **2009**, *324*, 71–74. [CrossRef] [PubMed]
31. Zitolo, A.; Goellner, V.; Armel, V.; Sougrati, M.-T.; Mineva, T.; Stievano, L.; Fonda, E.; Jaouen, F. Identification of catalytic sites for oxygen reduction in iron-and nitrogen-doped graphene materials. *Nat. Mater.* **2015**, *14*, 937–942. [CrossRef]
32. Chung, H.T.; Cullen, D.A.; Higgins, D.; Sneed, B.T.; Holby, E.F.; More, K.L.; Zelenay, P. Direct atomic-level insight into the active sites of a high-performance PGM-free ORR catalyst. *Science* **2017**, *357*, 479–484. [CrossRef]
33. Jaouen, F.; Proietti, E.; Lefèvre, M.; Chenitz, R.; Dodelet, J.-P.; Wu, G.; Chung, H.T.; Johnston, C.M.; Zelenay, P. Recent advances in non-precious metal catalysis for oxygen-reduction reaction in polymer electrolyte fuel cells. *Energy Environ. Sci.* **2011**, *4*, 114–130. [CrossRef]
34. Pan, F.; Jin, J.; Fu, X.; Liu, Q.; Zhang, J. Advanced oxygen reduction electrocatalyst based on nitrogen-doped graphene derived from edible sugar and urea. *ACS Appl. Mater. Interfaces* **2013**, *5*, 11108–11114. [CrossRef]
35. Hu, C.; Dai, L. Carbon-based metal-free catalysts for electrocatalysis beyond the ORR. *Angew. Chem. Int. Ed.* **2016**, *55*, 11736–11758. [CrossRef]
36. Byeon, A.; Yun, W.C.; Kim, J.M.; Lee, J.W. Non-precious Metal Catalysts for Two-Electron Oxygen Reduction Reaction. *ChemElectroChem* **2023**, *10*, e202300234. [CrossRef]
37. Chen, Z.; Higgins, D.; Yu, A.; Zhang, L.; Zhang, J. A review on non-precious metal electrocatalysts for PEM fuel cells. *Energy Environ. Sci.* **2011**, *4*, 3167–3192. [CrossRef]
38. Xia, D.; Tang, X.; Dai, S.; Ge, R.; Rykov, A.; Wang, J.; Huang, T.H.; Wang, K.W.; Wei, Y.; Zhang, K. Ultrastable Fe–N–C fuel cell electrocatalysts by eliminating non-coordinating nitrogen and regulating coordination structures at high temperatures. *Adv. Mater.* **2023**, *35*, e2204474. [CrossRef] [PubMed]
39. Yang, W.; Fellinger, T.-P.; Antonietti, M. Efficient metal-free oxygen reduction in alkaline medium on high-surface-area mesoporous nitrogen-doped carbons made from ionic liquids and nucleobases. *J. Am. Chem. Soc.* **2011**, *133*, 206–209. [CrossRef]
40. Ferrero, G.A.; Preuss, K.; Marinovic, A.; Jorge, A.B.; Mansor, N.; Brett, D.J.; Fuertes, A.B.; Sevilla, M.; Titirici, M.-M. Fe–N-doped carbon capsules with outstanding electrochemical performance and stability for the oxygen reduction reaction in both acid and alkaline conditions. *ACS Nano* **2016**, *10*, 5922–5932. [CrossRef] [PubMed]
41. Antolini, E. Carbon supports for low-temperature fuel cell catalysts. *Appl. Catal. B Environ.* **2009**, *88*, 1–24. [CrossRef]
42. Kim, S.; Park, S.J. A study on the role of carbon support materials for fuel-cell catalysts. In *Fuel Cell Research Trends*; Nova Science Publishers, Inc.: Hauppauge, NY, USA, 2007; pp. 411–443.
43. Fashedemi, O.O.; Bello, A.; Adebusuyi, T.; Bindir, S. Recent trends in carbon support for improved performance of alkaline fuel cells. *Curr. Opin. Electrochem.* **2022**, *36*, 101132. [CrossRef]
44. Pérez-Rodríguez, S.; Pastor, E.; Lázaro, M. Electrochemical behavior of the carbon black Vulcan XC-72R: Influence of the surface chemistry. *Int. J. Hydrogen Energy* **2018**, *43*, 7911–7922. [CrossRef]
45. Antxustegi, M.; Pierna, A.; Ruiz, N. Chemical activation of Vulcan® XC72R to be used as support for NiNbPtRu catalysts in PEM fuel cells. *Int. J. Hydrogen Energy* **2014**, *39*, 3978–3983. [CrossRef]
46. Higgins, D.C.; Meza, D.; Chen, Z. Nitrogen-doped carbon nanotubes as platinum catalyst supports for oxygen reduction reaction in proton exchange membrane fuel cells. *J. Phys. Chem. C* **2010**, *114*, 21982–21988. [CrossRef]
47. Cha, B.-C.; Jun, S.; Jeong, B.; Ezazi, M.; Kwon, G.; Kim, D.; Lee, D.H. Carbon nanotubes as durable catalyst supports for oxygen reduction electrode of proton exchange membrane fuel cells. *J. Power Sources* **2018**, *401*, 296–302. [CrossRef]
48. Liu, J.; Liu, S.; Yan, F.; Wen, Z.; Chen, W.; Liu, X.; Liu, Q.; Shang, J.; Yu, R.; Su, D. Ultrathin nanotube structure for mass-efficient and durable oxygen reduction reaction catalysts in PEM fuel cells. *J. Am. Chem. Soc.* **2022**, *144*, 19106–19114. [CrossRef]
49. Lawal, A.T. Recent application of carbon nanotubes in energy storage and conversion devices. *Carbon Trends* **2025**, *19*, 100470. [CrossRef]

50. Song, Y.; Qiu, S.; Feng, S.; Zuo, R.; Zhang, Y.; Jia, K.; Xia, X.; Chen, M.; Ji, K.; Wang, C. A review of carbon nanotubes in modern electrochemical energy storage. *New Carbon Mater.* **2024**, *39*, 1037–1074. [CrossRef]
51. Iijima, S.; Yudasaka, M.; Yamada, R.; Bandow, S.; Suenaga, K.; Kokai, F.; Takahashi, K. Nano-aggregates of single-walled graphitic carbon nano-horns. *Chem. Phys. Lett.* **1999**, *309*, 165–170. [CrossRef]
52. Ragupathy, P.; Bhat, S.D.; Kalaiselvi, N. Electrochemical energy storage and conversion: An overview. *Wiley Interdiscip. Rev. Energy Environ.* **2023**, *12*, e464. [CrossRef]
53. Serban, B.-C.; Bumbac, M.; Buiu, O.; Cobianu, C.; Brezeanu, M.; Nicolescu, C. Carbon nanohorns and their nanocomposites: Synthesis, properties and applications. A concise review. *Ann. Acad. Rom. Sci. Ser. Math. Appl.* **2018**, *11*, 5–18.
54. Zhu, S.; Xu, G. Single-walled carbon nanohorns and their applications. *Nanoscale* **2010**, *2*, 2538–2549. [CrossRef] [PubMed]
55. Karousis, N.; Suarez-Martinez, I.; Ewels, C.P.; Tagmatarchis, N. Structure, properties, functionalization, and applications of carbon nanohorns. *Chem. Rev.* **2016**, *116*, 4850–4883. [CrossRef]
56. Yudasaka, M.; Iijima, S.; Crespi, V.H. Single-wall carbon nanohorns and nanocones. In *Carbon Nanotubes: Advanced Topics in the Synthesis, Structure, Properties and Applications*; Springer: Berlin/Heidelberg, Germany, 2007; pp. 605–629.
57. Yaldagard, M.; Jahanshahi, M.; Seghatoleslami, N. Carbonaceous nanostructured support materials for low temperature fuel cell electrocatalysts—A review. *World J. Nano Sci. Eng.* **2013**, *3*, 121–153. [CrossRef]
58. Shao, Y.; Yin, G.; Gao, Y. Understanding and approaches for the durability issues of Pt-based catalysts for PEM fuel cell. *J. Power Sources* **2007**, *171*, 558–566. [CrossRef]
59. Galiote, N.A.; Oliveira, F.E.; de Lima, F.H.B. Nitrogen-Doped Carbon-Encapsulated FeCo Nanoparticles as Non-Noble Metal Cathode Electrocatalyst for Direct Formate Fuel Cells. In *Electrochemical Society Meeting Abstracts 231*; The Electrochemical Society, Inc.: Pennington, NJ, USA, 2017; p. 1448.
60. Yu, X.; Ye, S. Recent advances in activity and durability enhancement of Pt/C catalytic cathode in PEMFC: Part II: Degradation mechanism and durability enhancement of carbon supported platinum catalyst. *J. Power Sources* **2007**, *172*, 145–154. [CrossRef]
61. Jang, H.-W.; Lee, S.Y.; Lee, J.Y.; Joh, H.-I. Effect of Fe content on nonprecious cathodic catalysts derived from a metal–organic framework for direct ammonia fuel cells. *Carbon Lett.* **2023**, *33*, 215–223. [CrossRef]
62. He, J.; Zheng, T.; Wu, D.; Zhang, S.; Gu, M.; He, Q. Insights into the determining effect of carbon support properties on anchoring active sites in Fe–N–C catalysts toward the oxygen reduction reaction. *ACS Catal.* **2022**, *12*, 1601–1613. [CrossRef]
63. Shen, H.; Thomas, T.; Rasaki, S.A.; Saad, A.; Hu, C.; Wang, J.; Yang, M. Oxygen reduction reactions of Fe-NC catalysts: Current status and the way forward. *Electrochem. Energy Rev.* **2019**, *2*, 252–276. [CrossRef]
64. Zhou, Y.; Yu, Y.; Ma, D.; Foucher, A.C.; Xiong, L.; Zhang, J.; Stach, E.A.; Yue, Q.; Kang, Y. Atomic Fe dispersed hierarchical mesoporous Fe–N–C nanostructures for an efficient oxygen reduction reaction. *ACS Catal.* **2020**, *11*, 74–81. [CrossRef]
65. Liu, B.; Huang, B.; Lin, C.; Ye, J.; Ouyang, L. Porous carbon supported Fe-NC composite as an efficient electrocatalyst for oxygen reduction reaction in alkaline and acidic media. *Appl. Surf. Sci.* **2017**, *411*, 487–493. [CrossRef]
66. Kramm, U.I.; Herrmann-Geppert, I.; Fiechter, S.; Zehl, G.; Zizak, I.; Dorbandt, I.; Schmeißer, D.; Bogdanoff, P. Effect of iron-carbide formation on the number of active sites in Fe–N–C catalysts for the oxygen reduction reaction in acidic media. *J. Mater. Chem. A* **2014**, *2*, 2663–2670. [CrossRef]
67. Su, F.-C.; Chu, G.-Y.; Yang, H. Silver Nano-particles Modification Used as Cathode Catalysts to Enhance Anion Exchange Membrane Fuel Cells. *Electrochim. Acta* **2025**, *534*, 146544. [CrossRef]
68. Norizan, M.N.; Moklis, M.H.; Demon, S.Z.N.; Halim, N.A.; Samsuri, A.; Mohamad, I.S.; Knight, V.F.; Abdullah, N. Carbon nanotubes: Functionalisation and their application in chemical sensors. *RSC Adv.* **2020**, *10*, 43704–43732. [CrossRef]
69. Luo, X.; Rojas-Carbonell, S.; Yan, Y.; Kusoglu, A. Structure-transport relationships of poly (aryl piperidinium) anion-exchange membranes: Eeffect of anions and hydration. *J. Membr. Sci.* **2020**, *598*, 117680. [CrossRef]
70. Ahmed, D.S.; Haider, A.J.; Mohammad, M. Comparesion of functionalization of multi-walled carbon nanotubes treated by oil olive and nitric acid and their characterization. *Energy Procedia* **2013**, *36*, 1111–1118. [CrossRef]
71. Le, V.T.; Ngo, C.L.; Le, Q.T.; Ngo, T.T.; Nguyen, D.N.; Vu, M.T. Surface modification and functionalization of carbon nanotube with some organic compounds. *Adv. Nat. Sci. Nanosci. Nanotechnol.* **2013**, *4*, 035017. [CrossRef]
72. Truong, V.M.; Yang, M.-K.; Yang, H. Functionalized carbon black supported silver (Ag/C) catalysts in cathode electrode for alkaline anion exchange membrane fuel cells. *Int. J. Precis. Eng. Manuf.-Green Technol.* **2019**, *6*, 711–721. [CrossRef]
73. Milowska, K.Z.; Majewski, J.A. Functionalization of carbon nanotubes with $–CH_n$, $–NH_n$ fragments, –COOH and –OH groups. *J. Chem. Phys.* **2013**, *138*, 194704. [CrossRef]
74. Mananghaya, M.; Promentilla, M.A.; Aviso, K.; Tan, R. Theoretical investigation of the solubilization of COOH-functionalized single wall carbon nanotubes in water. *J. Mol. Liq.* **2016**, *215*, 780–786. [CrossRef]
75. Zhao, Z.; Yang, Z.; Hu, Y.; Li, J.; Fan, X. Multiple functionalization of multi-walled carbon nanotubes with carboxyl and amino groups. *Appl. Surf. Sci.* **2013**, *276*, 476–481. [CrossRef]
76. Jin, H.; Lee, S.; Sohn, Y.; Lee, S.H.; Kim, P.; Yoo, S.J. Capping agent-free synthesis of surface engineered Pt nanocube for direct ammonia fuel cell. *Int. J. Energy Res.* **2021**, *45*, 18281–18291. [CrossRef]

77. Lee, K.R.; Song, D.; Park, S.B.; Han, J.-I. A direct ammonium carbonate fuel cell with an anion exchange membrane. *RSC Adv.* **2014**, *4*, 5638–5641. [CrossRef]
78. Liu, Y.; Pan, Z.; Esan, O.C.; Huo, X.; Shi, X.; An, L. Development and performance evaluation of a passive direct ammonia fuel cell. *J. Power Sources* **2023**, *570*, 233057. [CrossRef]

Disclaimer/Publisher's Note: The statements, opinions and data contained in all publications are solely those of the individual author(s) and contributor(s) and not of MDPI and/or the editor(s). MDPI and/or the editor(s) disclaim responsibility for any injury to people or property resulting from any ideas, methods, instructions or products referred to in the content.